Jurnal Kejuruteraan SI 3(1) 2020: 95-101
https://doi.org/10.17576/jkukm-2020-si3(1)-15

Airflow Simulation and Measurement of Brake Wear Particle Emissions with a Novel Test Rig

A.B. Sanuddin[a,b*], S. Kosarieh[a], C.A. Gilkeson[a], P.C. Brooks[a] & D.C. Barton[a]

[a] *School of Mechanical Engineering, Institute of Design, Robotics and Optimisation, University of Leeds, United Kingdom*
[b] *School of Manufacturing Engineering, Universiti Malaysia Perlis, Malaysia*

**Corresponding author: mnasa@Leeds.ac.uk*

Received 04 December 2019, Received in revised form 27 March 2020
Accepted 20 April 2020, Available online 30 September 2020

ABSTRACT

Particle emissions generated by the braking systems of road vehicles represents a significant non-exhaust contributor. Fine particles such as these are transported through airborne routes. They are known to adversely affect human health and currently there are no policies in place to regulate them. Before this issue can be addressed, it is important to characterise brake wear debris which is the purpose of this study. A newly-developed test rig consisting of a closed but ventilated enclosure surrounds a brake dynamometer equipped with a cast iron rotor. A sampling probe was made in accordance with the isokinetic principles in order to withdraw a representative aerosol sample from the outlet duct. Measurements of real-time particulate numbers and mass distributions are recorded using a Dekati ELPI®+ unit and the brake materials were tested under drag-braking conditions. Prior to measurements, Computational Fluid Dynamics (CFD) simulations were performed to investigate the most suitable sampling points used in the experiments. Preliminary experimental results show that there is a noticeable increase in particle numbers, compared to background levels, with a corresponding change in the mass distribution; coarser particles become more prominent during these braking events. These results provide confidence in the performance of the test rig and its ability to measure airborne brake wear debris in order to compare emissions from various friction pairs.

Keywords: Non-exhaust emission; brake wear particle; test rig; CFD; particle size distribution

INTRODUCTION

Road vehicle particulate matter (PM) emission originating from both exhaust and non-exhaust sources is recognised as a major pollutant in the European Union (Wahlström and Olofsson 2014). The formation of PM in the atmosphere is known to adversely affect human health. From a historical point of view, much effort has been exerted to mitigate against PM pollution. In recent decades, stringent regulations regarding exhaust emissions have been established to reduce this pollution level. However, only exhaust emissions are properly regulated while those which are of a non-exhaust type are not currently regulated despite the fact that they are major contributors in many European cities (Perricone et al. 2016; Hooftman et al. 2018). Non-exhaust contributors include brake, tyre and road wear debris, in addition to resuspension of deposited road material (Padoan & Amato 2018). Among these sources, brake-related PM is increasingly recognised as a major contributor, particularly in urban areas where braking events occur more frequently (Grigoratos and Martini 2015). Furthermore both Garg et al. (2000) and Sanders et al. (2003) have highlighted that a significant proportion of brake PM is airborne with the former estimating that 35% of PM is airborne and the latter indicating 50%.

Numerous studies have reported the relationship between adverse health effects and the characteristics of PM. It was shown that the particle size of PM is an important factor in influencing how the particles are deposited in the respiratory system and subsequently affect human health (Pope III and Dockery 2006; Kumar et al. 2013). Samet et al. (2000) showed that the concentrations of PM in the environment may be associated with human mortality. There is consistent evidence linking the level of PM concentration with the mortality rate from cardiovascular and respiratory illnesses. Furthermore, the chemical composition of particles may also have similar effects on human health (Magari et al. 2002; Ostro et al. 2007). Toxic substances which typically include Fe, Cu, Ni, Cr, Zn, Al, Pb, Se, Pd and Mn are often discovered in PM. From the aforementioned effects, it is important to consider both size distributions and composition characteristics of brake wear debris.

Accurately measuring airborne brake PM in an open atmosphere is very challenging because of contamination from numerous other sources. Consequently, this paper focuses on real-time measurement of particulate numbers and mass distributions in a newly developed test chamber using a Dekati Electrical Low Pressure Impactor (ELPI®+).

In parallel, Computational Fluid Dynamics (CFD) simulations are performed to guide the experiments by identifying suitable locations for taking particulate samples

DYNAMOMETER EXTRACTION SYSTEM

In this study, the determination of brake emissions is properly conducted inside a laboratory with control of the environment. A test rig was developed based on an existing disc brake dynamometer which was fitted with a cast iron rotor and asbestos-free pads. This was enclosed within a custom-made hexahedral Perspex box which seals the air in the immediately vicinity of the brake assembly, keeping it separate from the laboratory. Airflow within the enclosure is controlled using a fan to deliver fresh air through an inlet duct, before it mixes within the enclosure and exits through an outlet duct. Inlet air is cleaned using HEPA and carbon activated filters and vented to the atmosphere at the outlet. The speed of the fan can be adjusted to create an air velocity in the range of 6 to 15 m/s at the velocity test point by controlling the fan setting.

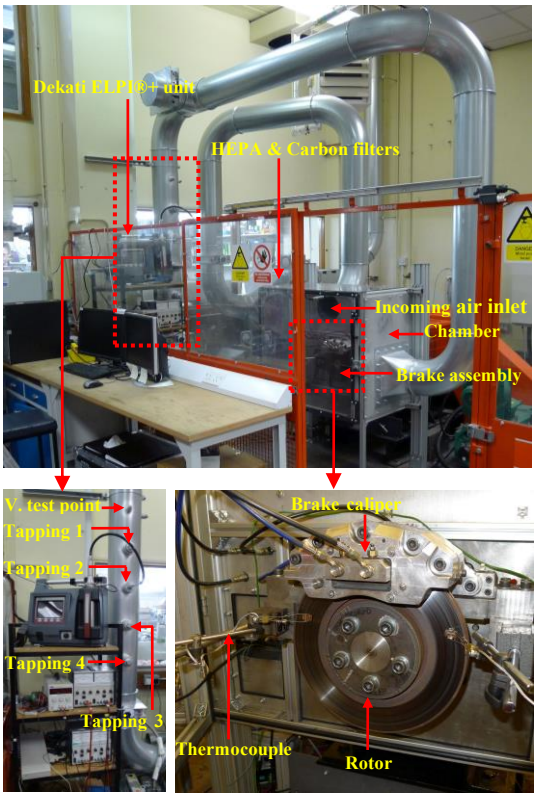

FIGURE 1. Photographs of the dynamometer extraction system

Within the sampling duct, four tappings (T1 – T4) and a velocity test point (VTP) were provided on the outlet duct for sampling brake PM as well as measuring airflow velocity, see Figure 1. A custom-made sampling probe was utilised at the T2 tap location to extract representative samples for analysis. An isokinetic sampling concept is applied to avoid biased results and errors. Therefore, the probe geometry and air sampling volume flow rate are tailored to comply with this concept. To measure and capture brake wear debris, the Dekati ELPI®+ particulate sampler is connected to the isokinetic probe using rubber hoses. The ELPI®+ unit allows measurement of airborne particle size distribution and concentration in real time with a sampling rate of 1 Hz or 10 Hz. The instrument measures particles in 14 size stages from 6 nm to 10 µm. The 14 impactor stages (including a back-up filter stage) make it possible to collect airborne particles on filters for gravimetric and chemical analyses. A sample flow rate of 10 litres/minute needs to be maintained for the unit to operate correctly.

ISOKINETIC SAMPLING METHOD

An isokinetic sampling concept was applied to the probe design in order to acquire reliable measurement data and avoid sampling errors. Isokinetic sampling occurs when the average air velocity through the sampling nozzle inlet is equal to the duct velocity at the same sampling point and the sampling probe is positioned parallel to the local free-stream. In addition, under isokinetic conditions the nozzle inlet should have a thin-walled, sharp-edged form in order to minimize air streamline distortion in the neighbourhood of the inlet (Belyaev and Levin 1974; Brockmann 2011; Hinds 1982). Accordingly, in the current study, the orientation of the sampling probe was aligned parallel to the free-stream and the probe geometry was tailored to achieve isokinetic conditions. An illustration of the sampling probe with the relevant dimensions is shown in Figure 2 (a). According to Belyaev and Levin (1974), a nozzle is considered as “thin-walled” when the ratio of the external tube diameter, D, to its internal diameter, d, satisfies the condition $D/d \leq 1.1$ regardless of the tube wall thickness to internal diameter ration, t/d, the angle of the tapered sample inlet, β and the Stokes number, Stk. Alternatively, the condition $D/d \geq 1.1$ should be satisfied if $t/d \leq 0.05$ and $\beta \leq 15^{o}$.

As mentioned above, the mean velocity at the test point (centre of the duct) was measured to be in the range of 6 – 15 m/s using an anemometer and since a Dekati ELPI®+ would be utilised, the airflow rate passing through the sampling probe should be equal to 10 litres/minute. From these two parameters, the internal diameter of the sampling probe, d, can be determined using the continuity equation.

By considering manufacturing constraints, a standard tube size that satisfies the abovementioned requirements should be selected. The chosen tube has an outer diameter of 1/4” (6.35 mm) and a wall thickness of 0.016” (0.4064 mm). A mean air velocity of 6.92 m/s was calculated in the centre of the ducting as well as the probe inlet. Since the chosen tube has the ratio of D/d equals to 1.15 and t/d is greater than 0.05, thus a Computational Fluid Dynamics simulation was performed to observe and evaluate the airflow behaviour at the sampling probe inlet. The results are elaborated in the next section. The full dimensions of the sampling probe chosen are shown in the Figure 2 (b).

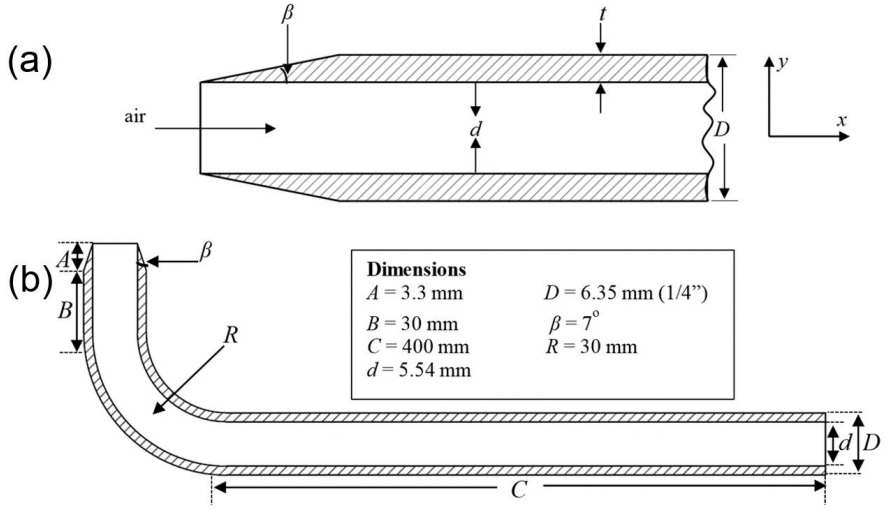

FIGURE 2. (a) Schematics of a thin-walled sampling probe & (b) Full dimensions of the sampling probe (not to scale).

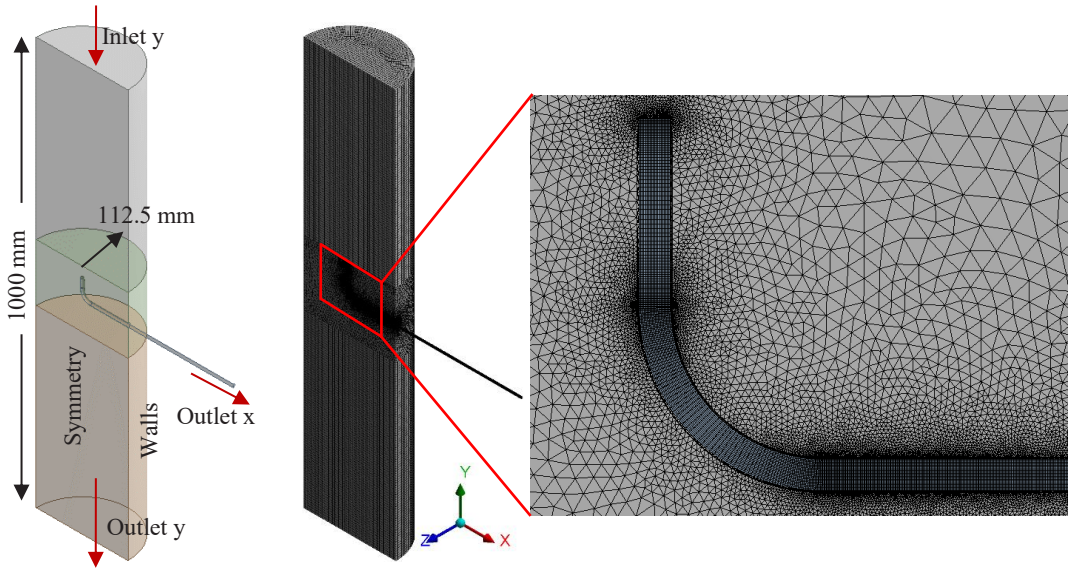

FIGURE 3. 3D schematic of the probe flow simulation and its domain with computational grid.

NUMERICAL METHODS

Two CFD simulations were performed in the present study. Firstly airflow through the dynamometer extraction system was simulated and the resulting flow patterns analysed. Secondly, a more detailed simulation of airflow through a segment of the duct containing sampling probe was considered, allowing airflow inside the probe itself to be evaluated. These two simulations were carried out using the commercial CFD software package, ANSYS Fluent (V16.2).

DUCTING AND ENCLOSURE SIMULATION

The main objective of the first simulation was to assess the behaviour of the airflow in the enclosed chamber and to predict the velocity profile in the vicinity of the sampling point. The inlet velocity to the chamber of 6.92 m/s and the pressure outlet of 1 atm were taken as the boundary conditions. The brake rotor was specified as a moving wall with a rotational speed of 135 rpm. The standard k-ε turbulence model with second order discretization schemes were set in Fluent. Standard (sea-level) atmospheric air properties which were from the Fluent database were used (density = 1.225 kg/m^3 and viscosity = 1.7894 x 10^{-5} kg/ms).

SAMPLING PROBE SIMULATION

The purpose of the second simulation was to examine the velocity profile in the vicinity of the sampling probe inlet. The inlet velocity was taken to be constant over the cross-section of the exhaust ducting and equal to 6.92 m/s. The pressure at the duct outlet was set to be 1 atm. To obtain the effect of the pump suction, a negative value of inlet velocity (-6.92 m/s) which is equivalent to the Dekati suction rate was applied to the outlet of the sampling probe. The standard k-ε turbulence model and air properties were applied as for the previous simulation. For a better illustration, a 3D schematic

of the simulation and its domain with computational grid are shown in Figure 3. The domain contains approximately 1.45 million elements which was obtained via a grid independence study.

NUMERICAL RESULTS

DUCTING AND ENCLOSURE SIMULATION

Figure 4 shows air pathlines passing through the dynamometer extraction system. The pathlines along the inlet duct are almost uniform and unidirectional before they are discharged into the enclosed chamber. Inside the chamber itself, the flow is complex and dominated by extensive mixing. The turbulence levels present around the brake assembly ensure that airborne particles generated from brake pads and the rotor are transported from the enclosure to the sampling location. It can be seen that the flow entering the chamber divides into two distinct streams, one circulating below the brake assembly and one above. Both streams then interact as they enter the outlet ducting. It is also noted that the flow of the air in the duct just after the chamber outlet is quite similar to flow behaviour at the inlet duct. A mild spiraling motion is evident suggesting that there is a rotational component about the duct axis which is likely due to the multiple bends along the outlet ducting.

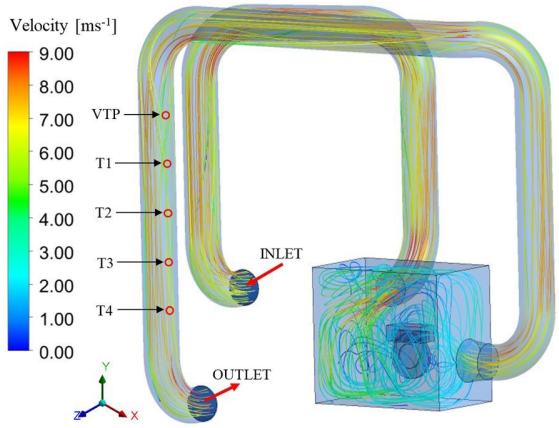

FIGURE 4. Air pathlines in the dynamometer extraction system.

To comprehend the velocity profile in the vicinity of the sampling tap locations and the velocity test point, velocity contours at these cross-sections are presented in Figure 5. They show that the velocity magnitude is somewhat higher in the left-hand side of the sampling duct. This might be caused by the preceding bend that the airflow has to follow; it naturally follows the outer radius of this relatively tight bend. When the airflow is downward, it was found that the high velocity region slowly diminishes such that a uniform velocity profile gradually develops. To obtain a better illustration of the velocity profile at the four tap locations and the velocity test point, a graph of the downward air velocity magnitude, U, against the duct width (denoted by the red lines in Figure 5) was plotted as shown in Figure 6. Overall, the shape of all profiles on the left-hand side is almost flat with a steep velocity gradient on the left-hand wall due to the no-slip boundary condition. However, on the right-hand side the velocity magnitude for all locations is noticeably reduced due to flow separation on the tight inner radius of the 90 degree elbow immediately above VTP. As the airflow reattaches, the velocity profile spanning the duct gradually becomes fuller and flatter as the airflow advances down towards the outlet.

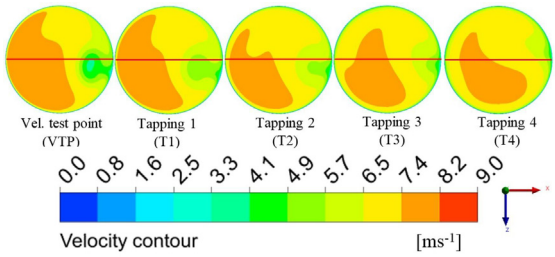

FIGURE 5. Resultant velocity contour at tapping and velocity test points.

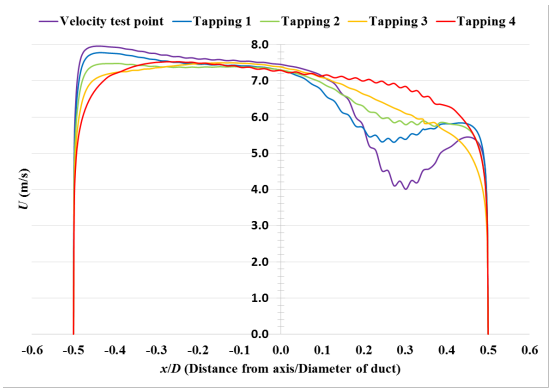

FIGURE 6. Radial velocity profile at tapping and velocity test points of the duct.

SAMPLING PROBE SIMULATION

Figure 7 shows a velocity magnitude contour map from the simulation of the airflow passing through and around the sampling probe. The velocity magnitude contours in Figure 7 are normalised by the free-stream velocity (taken as the inlet velocity). A close-up view of the contours is enlarged in the vicinity of the nozzle on the left-hand side of Figure 7, with the velocity profile plotted in the x-direction along the opening of the probe in Figure 8. It is important to note that there is a slight reduction in velocity at the two sides of the probe tip ($6.5 < U < 6.92$ m/s) compared to the velocity at the centre of the probe (~6.92 m/s); this is unavoidable and is due to the no-slip condition on the probe walls. Since the tip is shaped with knife edges, only a small distortion effect is evident which is limited to the vicinity of the probe tip circumference; flow in the centre of the probe is unaffected. It should be noted that if a significant reduction in velocity were to exist at the probe tip, deviation from the free-stream direction would be noticed. A consequence of this would be inaccurate wear debris particle samples which are taken from

the air entering the probe; this underlines the importance of careful probe positioning within the system and the results from the CFD simulation show that this has been achieved.

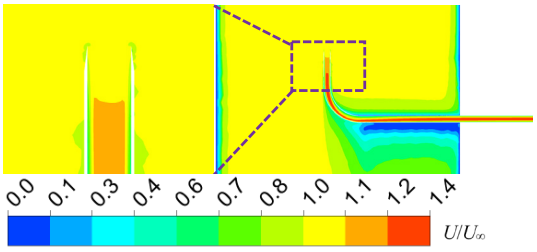

FIGURE 7. Velocity magnitude contours at the nozzle inlet.

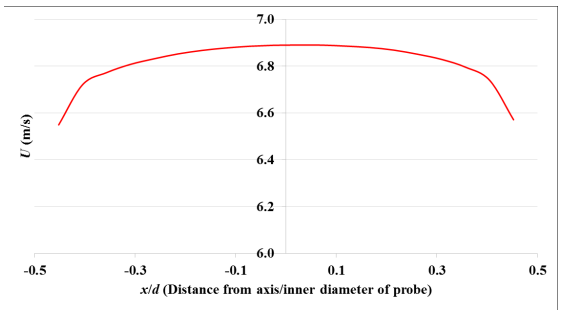

FIGURE 8. Magnitude of velocity profile at the inlet of the sampling probe.

BRAKE WEAR PARTICLE MEASUREMENT

Preliminary dynamometer tests were carried out prior to real-time particle measurements in order to determine the appropriate test parameters. Under drag brake conditions, the temperature of the rotor rubbing surface was recorded as rotational speed or hydraulic pressure were varied. The fan power was set at 5% of the total capacity in order to generate a velocity of ~7 m/s at the velocity test point. The duration of each test was 90 minutes to ensure that the rotor surface temperature reached a steady state. From the results, a constant rotor speed of 135 rpm was found to be suitable and three hydraulic brake pressures of 5, 10 and 15 bar were found to generate nearly constant temperatures of 200, 300 and 400°C respectively; these three conditions were selected to analyse brake wear debris. The temperature of the rotor rubbing surface is plotted as a function of time in Figure 9 and it is clear that steady-state conditions occur after about 3000 seconds for all three tests.

To investigate the role of the HEPA filter at the inlet duct, measurements of the background (laboratory) air and the air once inside the extraction system were carried out without running the dynamometer. The particle concentrations were measured using the Dekati unit over a duration of 10 minutes. It can be seen in Figure 10 that the particle concentrations for both measurements were approximately constant throughout each test. The laboratory background

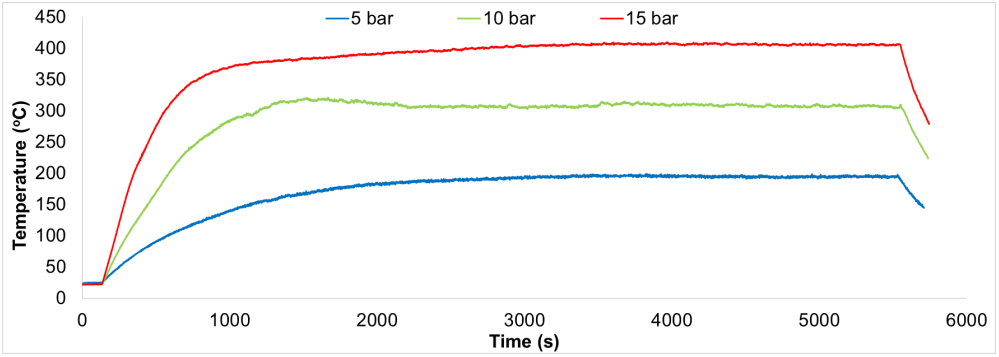

FIGURE 9. Rotor temperature variation with time for the three braking conditions at 135 rpm.

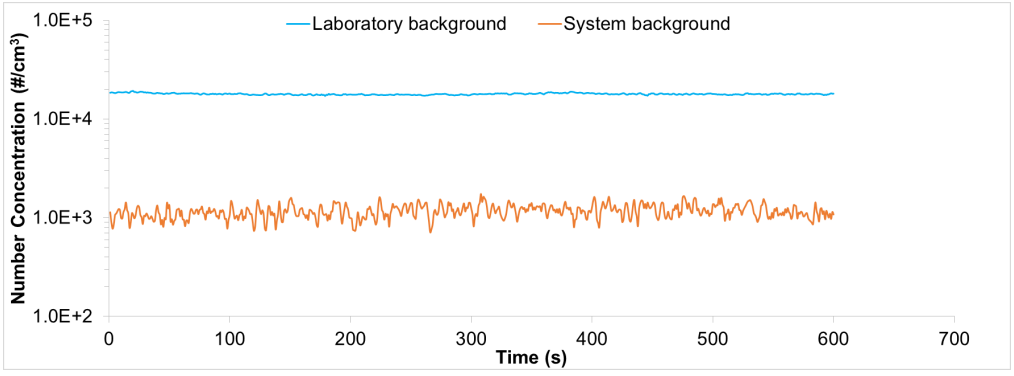

FIGURE 10. Comparison of particle concentrations in the laboratory and system environments.

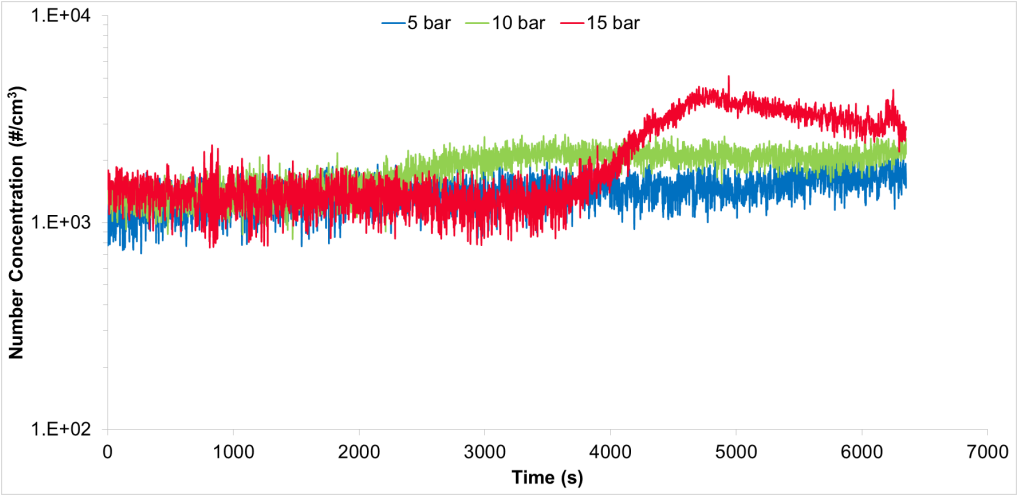

FIGURE 11. Particle concentration variation with time for the three tests at 135 rpm.

air recorded a higher concentration of particles compared to that inside the ducting system and so the application of the HEPA filter leads to a clean supply to the system. This result underlines the importance of filtering the air before it enters the dynamometer enclosure.

Measurements of particle concentration during the braking event were carried out for 90 minutes. Prior to these, the background level inside the system was measured at the beginning of the tests for 10 minutes in order to ensure the level of cleanness is consistent and acceptable. Three tests of 5, 10 and 15 bar at a constant speed of 135 rpm were employed in order to study the effect of the temperature on the particle concentration and mass distribution. As expected, it was found that the real time particulate numbers increase with time for all tests (see Figure 11). The test at the lowest brake pressure of 5 bar demonstrates an increasing pattern starting from 1000 seconds of the test duration although the increment is not considerable. The tests at 10 and 15 bar also show a similar trend but starting at 2000 and 4000 seconds in the test cycle, respectively. The particle concentration generally increases with hydraulic pressure. This may be caused by the different temperatures developed during the contact for the three conditions studied. It is postulated that brake materials soften due to the reduction in the bonding strength at elevated temperatures. Consequently, more brake particulates are generated with increasing brake rotor temperature.

Examining the results in more detail, Figure 12 shows the mass concentration distribution of the brake wear particles measured from the three tests. Each test was actually repeated three times and the variability is not too high. All mass distributions exhibit concentration peaks for particle diameters, D_p, of 4-10 µm. The mass distributions highlight a noticeable difference between background and brake application measurements, particularly for the coarse particle fractions. Generally speaking, the mass fraction of coarser particles marginally increases when the brake pressure decreases from 15 to 10 bar, at a constant speed of 135 rpm. However a much more significant increase occurs in the 4-10 µm range when the pressure is reduced to 5 bar. This may be because large particles are more readily released when the pad-rotor contact pressure is reduced. The higher the brake pressure, the stronger the brake pad squeezes on the brake rotor and the less possibility the particles to escape from the interface. Based on the results, it is estimated that approximately 90% of the total brake particulate mass is emitted as particle sizes in the 4 to 10 µm range for the conditions studied. This shows that coarse particles within this range dominate the brake wear debris emissions of road vehicles which agrees with previous studies (e.g. Sanders et al. 2003).

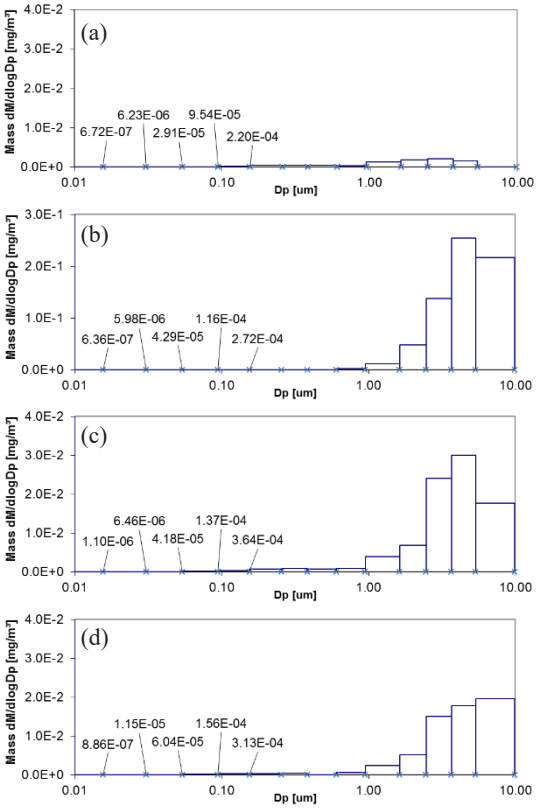

FIGURE 12. Mass distribution measurements for (a) background and (b,c,d) brake application at 5, 10 & 15 bar hydraulic pressure respectively.

CONCLUSION

This paper presents the design of a test rig for measuring airborne brake wear debris. An initial CFD simulation showed that a well-mixed flow pattern exists within the rig which would be expected to contain a wide range of airborne particles. In addition, the velocity profile on the left-hand side of the duct for all tappings is generally uniform and this suggests that the sampling point in this particular rig should be taken from this region, where the flow is more stable. The deviation between the inlet velocity to the chamber and the velocity at the centre of tapping locations was computed to be no greater than 8%. The second CFD simulation results show a small effect of distortion in the vicinity of the sampling probe inlet particularly around the tip. However this is not thought to be significant in terms of the operation of the sampling probe which is confirmed to achieve near isokinetic conditions. The findings from particulate measurements indicate that significant increases in wear debris emissions in the size range 4-10 µm occur when the brake is operating under drag braking conditions compared to the general background level. The mass fractions of coarse particles also increase significantly when the brake pressure is reduced to 5 bar which is more representative of normal city driving. Work is currently ongoing in this area.

DECLARATION OF COMPETING INTEREST

None.

ACKNOWLEDGEMENT

The lead author would like to thank the Malaysian government for the support provided.

REFERENCES

Belyaev, S.P. & Levin, L.M. 1974. Techniques for collection of representative aerosol samples. *Journal of Aerosol Science* 5: 325-338.

Brockmann, J.E. 2011. Aerosol transport in sampling lines and inlets. In: Kulkani, P., Baron, P. A. & Willeke, K. (eds.) *Aerosol Measurement: Principles, Techniques, and Applications*. Third edition. New Jersey: John Wiley & Sons, Inc..

Garg, B.D., Cadle, S.H., Mulawa, P.A., Groblicki, P.J., Laroo, C. & Parr, G.A. 2000. Brake Wear Particulate Matter Emissions. *Environmental Science & Technology* 34: 4463-4469.

Grigoratos, T. & Martini, G. 2015. Brake wear particle emissions: A review. *Environmental Science and Pollution Research* 22: 2491-2504.

Hinds, W.C. 1982. *Aerosol Technology: Properties, Behavior, and Measurement of Airborne Particles*. First edition. John Wiley & Sons.

Hooftman, N., Messagie, M., Van Mierlo, J. & Coosemans, T. 2018. A review of the European passenger car regulations - Real driving emissions vs local air quality. *Renewable and Sustainable Energy Reviews*. 86: 1-21.

Kumar, P., Pirjola, L., Ketzel, M. & Harrison, R.M. (2013) Nanoparticle emissions from 11 non-vehicle exhaust sources - a review. *Atmospheric Environment* 67: 252-277.

Magari, S.R., Schwartz, J., Williams, P.L., Hauser, R., Smith, T.J. & Christiani, D.C. 2002. The association of particulate air metal concentrations with heart rate variability. *Environmental Health Perspectives* 110: 875-880.

Ostro, B., Feng, W.Y., Broadwin, R., Green, S. & Lipsett, M. 2007. The effects of components of fine particulate air pollution on mortality in California: results from CALFINE. *Environmental Health Perspectives* 115: 13-19.

Padoan, E. & Amato, F. 2018. Chapter 2 - Vehicle Non-Exhaust Emissions: Impact on Air Quality. In: Amato, F. *Non-Exhaust Emissions*. First edition. Academic Press.

Perricone, G., Wahlström, J. & Olofsson, U. 2016. Towards a test stand for standardized measurements of the brake emissions. *Proceedings of the Institution of Mechanical Engineers, Part D: Journal of Automobile Engineering* 230: 1521-1528.

Pope III, C.A. & Dockery, D.W. 2006. Health Effects of Fine Particulate Air Pollution: Lines that Connect. *Journal of the Air & Waste Management Association* 56: 709-742.

Samet, J.M., Dominici, F., Curriero, F.C., Coursac, I. & Zeger, S.L. 2000. Fine particulate air pollution and mortality in 20 U.S. Cities, 1987-1994. *New England Journal of Medicine* 343: 1742-1749.

Sanders, P.G., Xu Ning, Dalka, T.M. & Maricq, M.M. 2003. Airborne Brake Wear Debris: Size Distributions, Composition, and a Comparison of Dynamometer and Vehicle Tests. *Environmental Science & Technology* 37: 4060-4069.

Wahlström, J. & Olofsson, U. 2014. A field study of airborne particle emissions from automotive disc brakes. *Proceedings of the Institution of Mechanical Engineers, Part D: Journal of Automobile Engineering* 229: 747-757.